6th IAHR International Meeting of the Workgroup on Cavitation and Dynamic Problems in Hydraulic Machinery and Systems, September 9-11, 2015, Ljubljana, Slovenia

SPACE-TIME DECOMPOSITION FOR ANALYZING FLUCTUATIONS IN FRANCIS TURBINES

Josselin GUILLOZET*

Alstom Hydro France, Grenoble, France

Alexandre DUPARCHY

Alstom Hydro France, Grenoble, France

Thomas DE COLOMBEL

Alstom Hydro France, Grenoble, France

ABSTRACT

The spatial harmonic decomposition (SHD) is a new analysis method that allows a broader perspective into the instabilities occurring in Francis turbines at off-design points. From a set of pressure signals distributed in space, this method offers an expansion of the pressure fluctuations into relevant patterns. It is a more robust and complete method than existing processes, that already distinguish between synchronous and asynchronous fluctuations.

Such methods and physical analyses allow a better understanding of Francis turbines behavior at part load and deep part load. Indeed Francis turbines are increasingly required to operate at off-design points to integrate intermittent renewable energy source into the electrical grid. In such conditions, the flow may be unstable and lead to strong fluctuations. A way to assess associated risks has long been to measure wall pressure fluctuations at different locations of the reduced scale turbine. However rough peak-to-peak levels of these pulsations do not tell much about the actual solicitations for the runner and which part of the fluctuation may be transposable to full scale machine.

After a short mathematical description of SHD, this paper will discuss its application to model Francis turbines.

KEYWORDS

Pressure Pulsations, Part Load, Deep Part Load, Francis Turbine, Stability, Vortex Rope, Hydro-acoustic Resonance

1. INTRODUCTION

Today, the stability of a turbine is mainly judged on reduced scale model by analyzing peak-to-peak value of pressure pulsations measurements. The sensors are commonly located at the spiral case inlet, in the vaneless area and in the draft tube. For a given net head, these peak-to-peak values are then expressed as a percentage of the net head against the power output and supposed to transpose as such to the full scale machine. Such a rough peak-to-peak analysis illustrated on Fig. 1 suffers at least two major drawbacks.

* *Corresponding author:* Alstom Hydro France, 82 Av. Léon Blum - BP 75,38041 Grenoble Cedex 9, France, phone: +33 4 76 39 28 46, email: josselin-a.guillozet@power.alstom.com

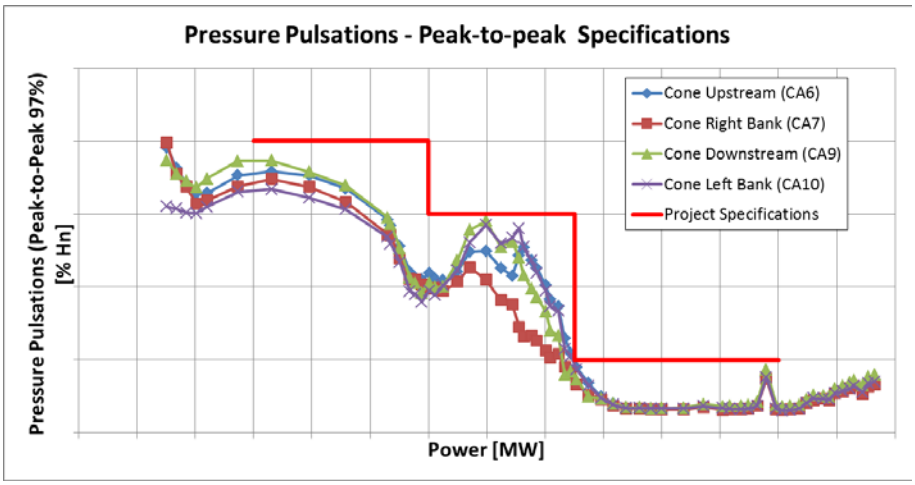

Fig. 1 Traditionnal specifications in terms of peak-to-peak

Firstly, it does not tell whether the pulsations will actually decrease the lifetime of components or induce power fluctuations. For the same peak-to-peak value of pressure pulsations, a synchronous instability (as defined in [3]) and a rotating pattern may have very different impacts. The left chart of Fig. 2 shows that synchronous resonances are often not visible in the runner strain fluctuations contrary to the rotating vortex rope. On the other side, synchronous instabilities usually generate more power fluctuations than rotating patterns as illustrated on the right chart of Fig. 2.

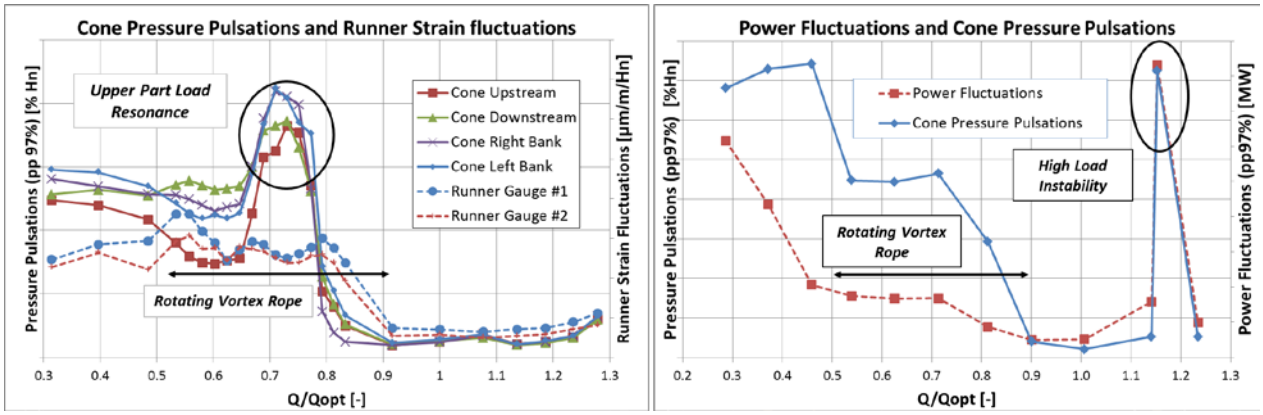

Fig. 2 Left, strain fluctuations in a reduced scale runner and cone pressure pulsations. Right, power and pressure pulsations on a full scale turbine before enabling mitigation device from [6].

Secondly, peak-to-peak analysis does not make any difference between phenomena that transpose more or less easily to the full scale turbine. For example, hydro-acoustic resonances may depend on the distance between the upstream and downstream tanks, which is not always in homology from the reduced scale to the full scale turbine. Furthermore, resonances are very sensitive to the cavitation volume and hence to both Thoma and Froude similitude. Unfortunately, Froude similitude is not always compatible at reduced scale with range of Reynolds numbers required for the transposition of losses to full scale turbine.

The SHD solves these problems by making visible the space shape of pressure pulsations on any cross section. Indeed, thanks to this method, synchronous pulsations and various rotating pattern are separated. Once each cross section is analyzed, SHD patterns may be combined to exhibit spatial shape in the third dimension: from the inlet to the outlet of the turbine.

After a short review of the mathematical properties of the SHD first developed in [1], this paper will discuss its application to common pressure pulsation measurements on Francis turbines.

2. SHD MATHEMATICAL PROPERTIES

The details of the mathematical development for the SHD may be found in [1]. This paragraph gives the main properties of this method.

The pressure p is considered on a circle perpendicular to and centered on the runner axis. Such a circle may be defined on a draft tube cross section or on a ring above or below the vaneless area. On this circle, the pressure is only function of time t and of the azimuth α.

The periodicity of $p(\alpha, t)$ in variable α allows an expansion into a Fourier series. Then, on top of this first expansion for the spatial variable, a more common Fourier transform is applied for the time t. This double Fourier expansion leads to following final decomposition:

$$p(\alpha,t) = \int_{\omega=0}^{\infty} A_{0,\omega}\cos(\omega t + \phi_{0,\omega})\,d\omega + \sum_{k=+1}^{k=+\infty}\int_{\omega=0}^{\infty} A_{k,\omega}\cos(k\alpha - \omega t + \phi_{k,\omega})\,d\omega + \sum_{k=-\infty}^{k=-1}\int_{\omega=0}^{\infty} A_{k,\omega}\cos(k\alpha - \omega t + \phi_{k,\omega})\,d\omega \quad (1)$$

Each of these terms has the following physical interpretation:

- $\boldsymbol{P_{0,\omega}(t) = A_{0,\omega}\cos(\omega t + \phi_{0,\omega})}$ is a synchronous pattern. If sensors are equally distributed, it is the space average of all the sensors.
- $P_{k,\omega}(t) = A_{k,\omega}\cos(k\alpha - \omega t + \phi_{\omega,t})$ with $k > 0$ is a rotating pattern with k nodal diameter(-s). The pattern rotates in the direction of $\alpha > 0$ with angular velocity $\dot{\alpha} = \omega/k$.
- $P_{k,\omega}(t) = A_{k,\omega}\cos(k\alpha - \omega t + \phi_{\omega,t})$ with $k < 0$ is a pattern with k nodal diameter(s) rotating in the opposite direction.

Some of these patterns are pictured on Fig. 3 together with corresponding time series on four equally distributed sensors.

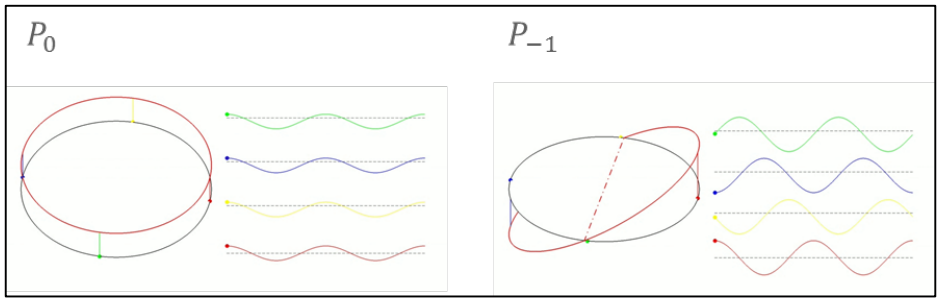

Fig. 3 Illustration of the two most common P_k patterns to be found in a Francis turbine.Corresponding time series from 4 sensors on the right of each pattern.

In practice, the time is acquired at a limited sampling frequency f_s. Likewise, regarding the space variable α, a limited number N_α of sensors are installed. According to Nyquist-Shannon theorem, a sampling frequency f_s gives only access to phenomena up to a frequency $f_{\max} = f_s/2$. Higher frequency will experience aliasing, that is, they will be mistaken for lower frequency.

Similarly, N_α gives only access to patterns up to $k_{max} = \pm N_\alpha/2$. In the next paragraph, every time SHD is applied, 3 or 5 sensors have been used, giving access to patterns having up to 1 or 2 nodal diameter. Pattern with a number of nodal diameters $|k|$ higher than $N_\alpha/2$ will be seen as a pattern with the parameter:

$$k_{measured} = k_{real} \text{ modulo } N_{alpha} \qquad (2)$$

For example, if only N_α =5 sensors are available, the passage of 15 blades in the vaneless area expected to be mainly seen on $P_{-15,real}$ will be captured by $P_{0,measured}$, because $-15 = -3 \times 5 + 0$. It should be noted that not only SHD but all methods exploring the spatial shape of fluctuations will experience aliasing but SHD provides the mathematical framework to explain it.

To quantify the relative contribution of each pattern to the overall signal, Parseval's theorem may be invoked on signal powers. Total signal power of the fluctuations on a section may be defined as:

$$Power(p) = \underbrace{\frac{1}{2\pi}\int_{-\pi}^{\pi}\left(\frac{1}{T}\int_{t=0}^{T} p^2(\alpha,t)dt\right)d\alpha}_{\text{Total Signal Power}} = \sum_{k=-\infty}^{k=+\infty}\int_{\omega=0}^{\infty} \underbrace{\frac{1}{2}A_{k,\omega}^2}_{\substack{\text{Contribution}\\ \text{of one single}\\ \text{pattern}}} d\omega \qquad (3)$$

After spatial discretization with $\boldsymbol{N_\alpha}$ sensors and introduction of Root-Mean-Square (RMS) over time or frequency:

$$Power(p) = \underbrace{\frac{1}{N_\alpha}\sum_{i=1}^{N_\alpha} RMS^2(p_i)}_{\text{Total Signal Power}} = \sum_{k=-k_{max}}^{k=+k_{max}} \underbrace{RMS^2(P_k)}_{\substack{\text{Contribution}\\ \text{of one single}\\ \text{pattern}}} \qquad (4)$$

It allows one to answer the question: what is the contribution of each pattern to the overall signal?

3. APPLICATION TO A FRANCIS TURBINE

The investigated case is a reduced scale model of a medium head Francis turbine. The runner has $Z_b = 15$ blades. Two load variations at a constant net head and constant runner speed f_0 have been performed from speed-no-load to very high load for two different Thoma numbers σ_{high} and σ_{low}. One sensor is located at the spiral case inlet. Three sensors are equally distributed on a circle at the top of the vaneless area between the wicket gate and the runner inlet. Five sensors are located in the cone below the runner outlet. σ_{high} is a high Thoma number which gives little cavitation and which is not representative of a full scale machine. However, operating points at σ_{high} may be compared with single-phase flow numerical calculation. Load variation with σ_{low} is more representative of a real plant downstream level and exhibits resonances and instabilities that are strongly dependent on the cavitation volume in the draft tube.

On Fig. 4, the total signal power is plotted for both the vaneless area and the cone against the discharge Q nondimensionalized by the optimum discharge Q_{opt}. Some time series and spectra are also given for a selection of four operating points on Fig. 5.

In-phase patterns P_0 are pictured on Fig. 6. They highlight:

1. Small resonances at partial load (e.g. OP3): two resonant frequencies can be seen at $f_{r1} = 0.4f_0$ (very close to the vortex rope second harmonic) and $f_{r2} = 1.2f_0$. They are present everywhere in the turbine. Such resonances were investigated recently in [4]. They are natural hydro-acoustic modes whose frequency and spatial shape depend mainly on the turbine length and on the cavitation volume. Some of these modes are probably excited by the vortex rope interacting with the draft tube elbow.

2. Small high load instabilities (OP4): One of them is here visible at frequency $f_{HLI} = 0.6f_0$. This kind of self-excited oscillation is due to the interaction between the runner and the cavitation volume in the draft tube. It is described for example in [5]. Like the resonances, it oscillates in phase everywhere in the turbine (see Fig. 5).
3. A small P_0 contribution by the helical vortex at partial load due to the elbow as identified in [2].

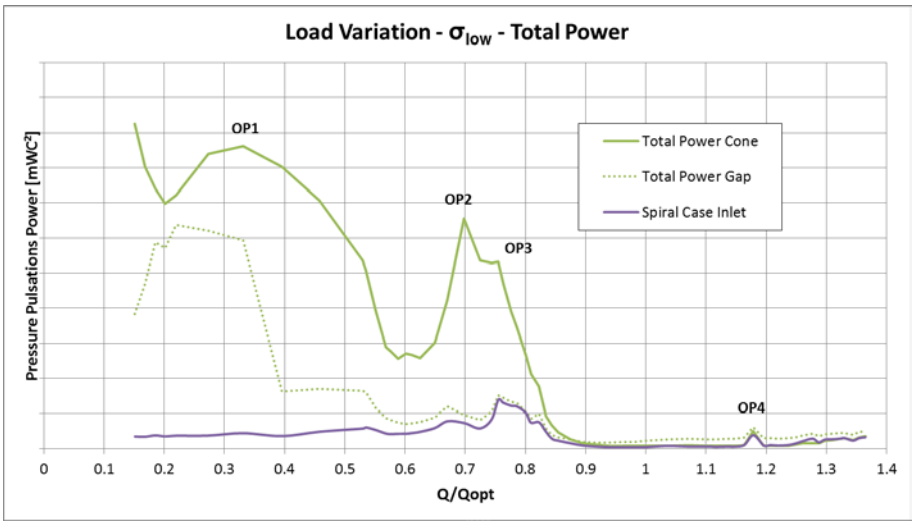

Fig. 4 Total signal power for draft tube and vaneless area sections. Unfiltered data for the spiral case inlet is also pictured. Four interesting operating points are labeled for discussion.

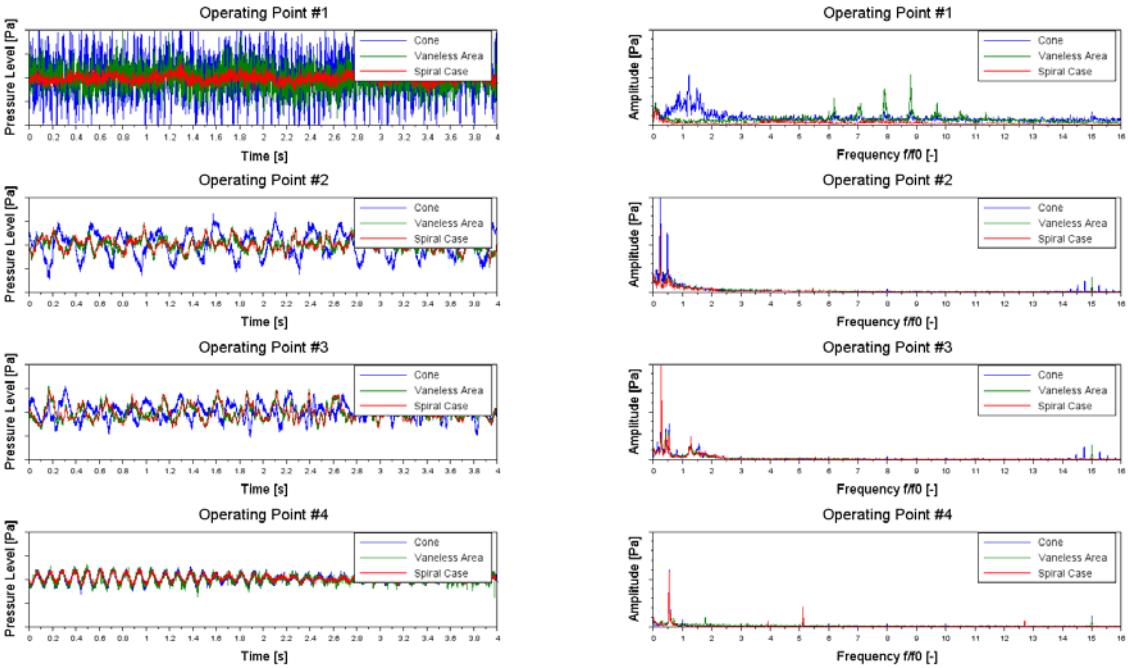

Fig. 5 Time series and corresponding FFT spectrum for interesting operating points labeled on Fig. 4. Amplitude scales are conserved from one OP to the other.

At deep partial load (below 0.6Qopt and before speed-no-load), part of the power of P_0 may be due to the aliasing of rotating patterns with a number of nodal diameter multiple of 5. Such patterns are probable, for example in the draft tube where five vortices may appear. More sensors on the same section would have allowed a better identification.

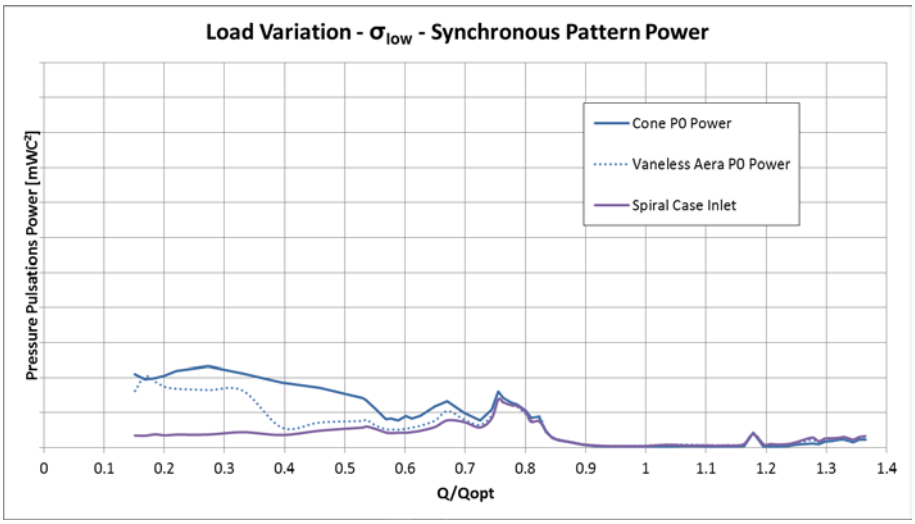

Fig. 6 Signal power of synchronous patterns from SHD for draft tube and vaneless area sections. Unfiltered data for the spiral case inlet is also pictured.

Rotating patterns P_k are plotted on Fig. 7. They are due to vortices rotating in the draft tube or to oscillating flow located in the vaneless area. They are related to a convective peripheral velocity V_u at radius R that drives their angular velocity $\dot{\alpha} \approx V_u/R$.

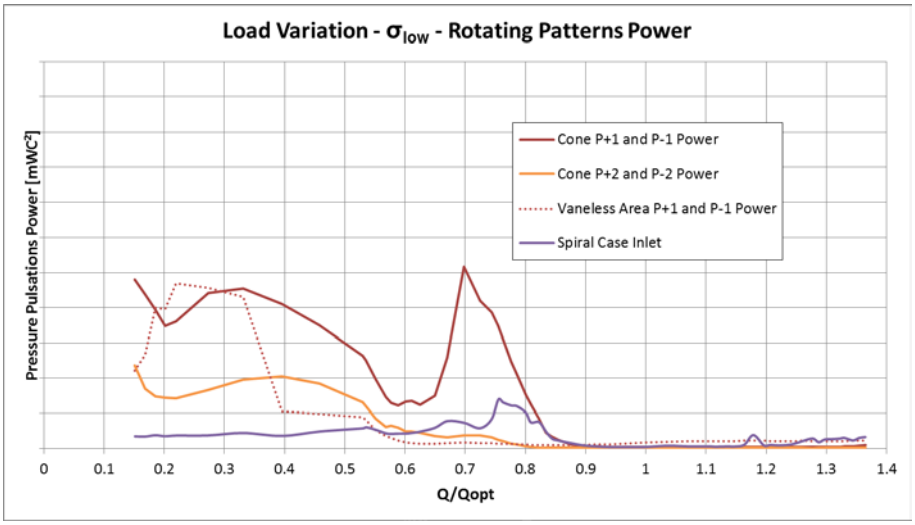

Fig. 7 Signal power of rotating patterns from SHD for draft tube and vaneless area sections. Unfiltered data for the spiral case inlet is also pictured.

Between 0.6Qopt and 0.9Qopt, the well-known helical vortex rope present on every Francis draft tube is captured mainly by a P_{-1} pattern plotted in red line. Its main frequency is $f_{VR} = 0.25f_0$. When the vortex gets closer to the cone wall for lower discharge, a second harmonic $2f_{VR}$ appears that is captured by a small P_{-2} pattern.

At deep partial load, the situation is less obvious but some interpretations can be made. Below 0.55Qopt, inter-blade vortices (IBV) are the main cavitating phenomenon visible inside the runner. In the stationary frame, their expected frequency signature might range from $0.2\mathrm{Z_b f_0} = 3f_0$ (15 vortices convected like the partial load vortex rope) to $\mathrm{Z_b f_0}$ (15 vortices precessing at runner speed). Fluctuations above $5\mathrm{f_0}$ are actually recorded mainly by pressure sensors in the vaneless area below 0.4Qopt (see Fig. 5). In this particular turbine, they may be good candidates to be signatures of IBV. In the cone, mainly frequencies below $3f_0$ can be observed. These frequencies may be interpreted in the continuity of the range 0.6-0.9Qopt as 1 to 5 rotating vortices similar to the helical vortex rope. Nevertheless these vortices are not

stable and the number of them may change over time at the same operating point. Time-frequency or time-SHD analysis should support this affirmation. Contrary to the helical vortex rope, draft tube vortices at deep part load seem to only have a local impact confined to the draft tube itself.

Finally, pressure sensors in the cone are of little use to investigate what happens in the runner at deep part load. Vaneless area measurements seem to be a bit more meaningful to assess risks due to IBV. Nevertheless, fluctuations may have been harmful for the runner before their detection in the vaneless area. Therefore, only on-board measurements may decide about the actual risk for the runner.

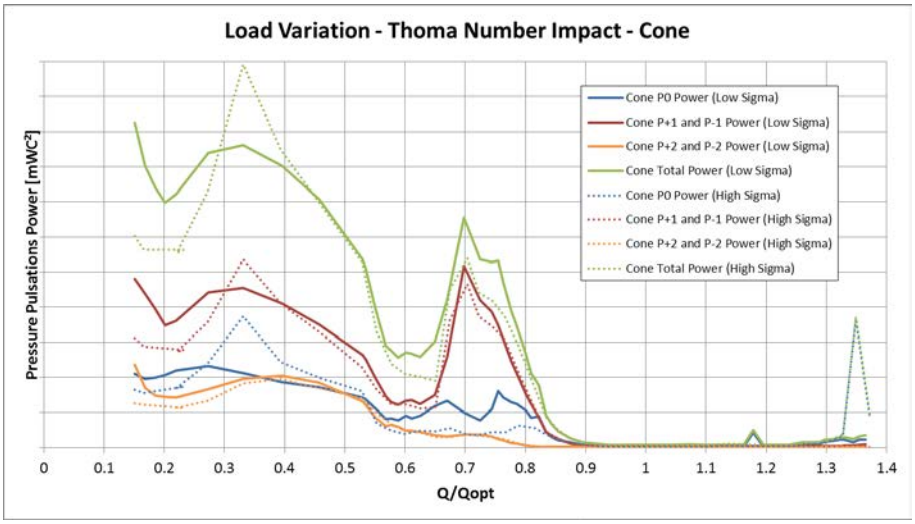

Fig. 8 Impact of Thoma number on SHD patterns for two Thoma numbers

Another aspect that supports the separation of synchronous from rotating patterns is their respective sensitivity to the Thoma number. This property is illustrated on Fig. 8 with dotted curves for the lower Thoma number. Rotating patterns related mainly to flow convection are little impacted by a change in the counter-pressure (red and orange curves) on a broad operating range. On the contrary, partial load resonances and high load instabilities which strongly depend on the cavitation volume, change much more with the Thoma number (blue curves).

4. CONCLUSION

Spatial Harmonic Decomposition was applied to pressure pulsations on a Francis turbine. Thanks to this space-time decomposition, unstable hydraulic phenomena are easily identified and their contribution to the overall fluctuations is well quantified. It is a powerful alternative to peak-to-peak analysis and project specifications would be more suitably express in terms of SHD patterns power. Once phenomena have been identified on a reduced or an existing full scale machine, they can be addressed with the appropriate mitigation measure.

The next step would consist in applying the SHD to a network of pressure sensors inside the runner to have a better insight of the phenomena at deep part load. Indeed, common pressure sensors in the vaneless area and in the draft tube fail to deliver a clear view of what happens at such operating points.

5. REFERENCES

[1] Duparchy A, Guillozet J, de Colombel T and Bornard L: Spatial Harmonic Decomposition as a tool for unsteady flow phenomena analysis *27th IAHR Symposium on Hydraulic Machinery and Systems (IAHR). 2014.*

[2] Nishi M, Matsunaga S, Kubota S and Senoo Y: Surging Characteristics of conical and elbow-type draft tubes. *IAHR Section Hydraulic Machinery, Equipment and Cavitation, 12th Symp. (Stirling, UK).* 1984.

[3] Doerfler P K: System dynamics of the Francis turbine half-load surge. *IAHR Section Hydraulic Machinery, Equipment and Cavitation, 11th Symp. (Amsterdam, Netherlands).* 1982.

[4] Favrel A, Landry C, Mueller A, Yamamoto K and Avellan F. Hydro-acoustic resonance behavior in presence of a precessing vortex rope: observation of a lock-in phenomenon at part load Francis turbine operation. *27th IAHR Symposium on Hydraulic Machinery and Systems (Montreal, Canada).* 2014.

[5] Mueller A, Favrel A, Landry C, Yamamoto K and Avellan F: On the physical mechanisms governing self-excited pressure surge in Francis turbines. *27th IAHR Symposium on Hydraulic Machinery and Systems (Montreal, Canada).* 2014.

[6] Flores E, Bornard L, Tomas L, et al. : Design of large Francis turbine using optimal methods. *26th IAHR Symposium on Hydraulic Machinery and Systems (Beijing, China).* 2012.

6. NOMENCLATURE

p	(Pa)	Pressure	k	(-)	Number of diametric node
α	(rad)	Spatial azimuth	$P_{k,\omega}$	(Pa)	Single SHD pattern
$A_{k,\omega}$	(Pa)	Pressure signal amplitude of a SHD pattern	$\phi_{k,\omega}$	(rad)	Phase of a SHD pattern
ω	(rad/s)	Time pulsation	ω_0 or f_0	(rad/s or Hz)	Runner rotation speed
N_α	(-)	Number of sensors on a cross-section	Z_b	(-)	Runner blade number
Q	(l/s)	Flow Rate	σ	(-)	Thoma number
$\dot{\alpha}$	(rad/s)	Angular rotation speed	V_u	(m/s)	Peripheral velocity
R	(m)	Radius			